

# The 130 GeV gamma-ray line and Sommerfeld enhancements

Jing Chen<sup>\*</sup> and Yu-Feng Zhou<sup>†</sup>

*State Key Laboratory of Theoretical Physics,  
Kavli Institute for Theoretical Physics China,  
Institute of Theoretical Physics, Chinese Academy of Sciences,  
Beijing, 100190, China*

## Abstract

Recently, possible indications of line spectral features in the Fermi-LAT photon spectrum towards the galactic center have been reported. If the distinct line features arise from dark matter (DM) annihilation into  $\gamma X$  ( $X = \gamma, Z^0$  or  $h^0$ ), the corresponding annihilation cross-section is unnaturally large for typical loop-induced radiative processes. On the other hand, it is still too small to be responsible for the observed DM relic density. We show that the mechanism of Sommerfeld enhancement with scalar force-carrier can provide a simple solution to these puzzles. The possibly large Sommerfeld enhancement of the cross-section for  $s$ -wave DM annihilation can significantly reduce the required effective couplings between DM and charged particles in typical loop diagrams. The DM particles necessarily annihilate into scalar force-carriers through tree-level  $p$ -wave process, which can dominate the total DM annihilation cross-section at freeze out, resulting in the correct thermal relic density, but has subdominant contributions to the DM annihilation today due to velocity suppression. We perform detailed analysis on the effects of  $p$ -wave Sommerfeld enhancement on freeze out. The results show that with the constraints from the thermal relic density, the required effective couplings can be reduced by an order of magnitude.

---

<sup>\*</sup>Email: jchen@itp.ac.cn

<sup>†</sup>Email: yfzhou@itp.ac.cn

# 1 Introduction

It has been well-established from observations that dark matter (DM) contributes to nearly 23% of the energy budget of the Universe. The leading DM candidates such as the weakly interacting massive particles (WIMPs) can interact weakly with the ordinary matter and possibly be detected through direct and indirect searches. Monoenergetic gamma-ray lines are one of the smoking gun signals of halo DM annihilation, which is hard to mimic by astrophysical sources.

Recently, a possible line spectral feature around 130 GeV or with an additional line at 111 GeV in the Fermi-Large-Area-Telescope (Fermi-LAT) photon spectrum in regions close to the galactic center (GC) have been reported [1–5]. Indications of similar spectral features have been reported in the galactic clusters with modest statistical significance [6] and possibly in unassociated gamma-ray point sources [7–10]. The latest analysis from Fermi-LAT collaboration also shows the indication of such line feature at 130 GeV (135 GeV) with 4.01 (3.35)  $\sigma$  local significance using unprocessed (reprocessed) data [11]. However, no globally significant gamma-ray line features have been established from the analysis of Fermi-LAT collaboration. It remains to be confirmed whether these line features are indeed from DM annihilation or due to instrumental uncertainties [12] or astrophysical backgrounds [13–15]. The upcoming HESS-II experiment can provide an independent check on existence of the gamma-ray line features.

The monoenergetic gamma-ray lines naturally arise from DM annihilation into two-body final states  $\gamma X$ , where  $X$  stands for the Standard Model (SM) neutral particles  $\gamma$ ,  $Z^0$  and Higgs boson  $h^0$  etc.. In this case, the energy of the photon is given by  $E_\gamma = m_\chi[1 - m_X^2/(4m_\chi^2)]$ , where  $m_\chi$  is the DM mass. The observed line signals correspond to a thermally averaged cross section multiplied by relative velocity  $\langle\sigma_{\gamma\gamma}v_{\text{rel}}\rangle \sim 1.27 \times 10^{-27} \text{ cm}^3\text{s}^{-1}$  for Einasto profile and  $\sim 2.27 \times 10^{-27} \text{ cm}^3\text{s}^{-1}$  for a generalized Navarro-Frenk-White (NFW) profile respectively [2]. Although the line spectral feature is expected from DM two-body annihilation, the corresponding cross-section and non-observation of an excess of accompanying continuum gamma-ray flux may challenge the explanation in terms of simple WIMP models [16–18]. First, in most DM models the DM-photon couplings are generated radiatively through loop level diagrams with charged intermediate states  $F\bar{F}$  where  $F$  can be SM charged gauge bosons  $W^\pm$  and charged fermions  $f$  except for the top-quark. For an annihilation cross-section  $\langle\sigma_{\gamma\gamma}v_{\text{rel}}\rangle \approx \mathcal{O}(10^{-27}) \text{ cm}^3\text{s}^{-1}$ , the required DM couplings to mediator particles are in general unnaturally large, which may raise the question of perturbativity [16]. Second, if the intermediate charged states are kinematically allowed to be the annihilation final states such as  $f\bar{f}$  and  $W^\pm W^\mp$ , the corresponding tree level cross-sections are related to that of DM annihilation into  $2\gamma$  as  $\langle\sigma_{f\bar{f}, WW}v_{\text{rel}}\rangle/\langle\sigma_{\gamma\gamma}v_{\text{rel}}\rangle \sim (\pi/\alpha_{\text{em}})^2 \approx 2 \times 10^5$ . Such

a large cross-section is stringently constrained by the non-observation of any excesses in the continuum gamma-ray spectrum and the cosmic-ray antiproton flux [19–23]. Finally, if the  $\chi\bar{\chi} \rightarrow F\bar{F}$  channels are not opened and  $\chi\bar{\chi} \rightarrow \gamma X$  is the main DM annihilation channel as suggested by the current observations, the corresponding cross-section is not large enough to generate the correct DM thermal relic density which typically requires  $\langle\sigma v_{\text{rel}}\rangle_F \approx 3 \times 10^{-26} \text{ cm}^3\text{s}^{-1}$  for  $s$ -wave annihilation.

Several mechanisms have been proposed to address this problem such as co-annihilation, forbidden channel, asymmetric DM [17], resonant annihilation and cascade annihilation [18], etc.. Note that many of them introduce degeneracies in the mass of the DM particles and the intermediate particles. Specific models in which the signals of  $\chi\bar{\chi} \rightarrow \gamma X$  and the thermal relic density are not correlated have been considered in Refs. [24–33].

In this work, we show that the Sommerfeld enhancement with *scalar* force-carrier can simultaneously explain the large loop level cross-sections and the correct thermal relic density without introducing degeneracies in the mass of the DM and mediator particles. In the presence of Sommerfeld enhancement, the cross-section for  $s$ -wave annihilation  $\chi\bar{\chi} \rightarrow \gamma X$  today can be greatly enhanced due to the multiple exchange of a light force-carrier  $\phi$ , which reduces the required couplings in the loop diagrams. As the force-carriers are light, the DM particles necessarily annihilate into the force-carriers. For  $\phi$  being a scalar particle, the annihilation  $\chi\bar{\chi} \rightarrow \phi\phi$  proceeds through  $p$ -wave. The  $p$ -wave process is also Sommerfeld enhanced, which can dominate the total annihilation cross-section at freeze out, lead to the correct thermal relic density, but plays a subdominant role in the halo DM annihilation today due to the velocity suppression. The total annihilation in the halo can be dominated by  $\gamma X$  channel, which can explain both the reported gamma-ray line spectrum and the nonobservation of continuum spectrum.

This paper is organized as follows. In Sec. 2, we begin with a brief review on the main features of the Sommerfeld enhancement, and then focus on the Sommerfeld enhancement of  $p$ -wave processes and its impact on the thermal relic density. The effects of kinetic decoupling for  $p$ -wave processes are also discussed. In Sec. 3, we discuss the maximally allowed Sommerfeld enhancement factor after considering the constraints from the thermal relic density for the case with scalar force-carriers. In Sec. 4, we apply the mechanism to a reference DM model in which the  $\chi\bar{\chi} \rightarrow 2\gamma$  proceeds through one-loop diagrams and discuss reduction of the required effective couplings between DM particles and the charged intermediate states in the loop. The conclusions are given in Sec. 5.

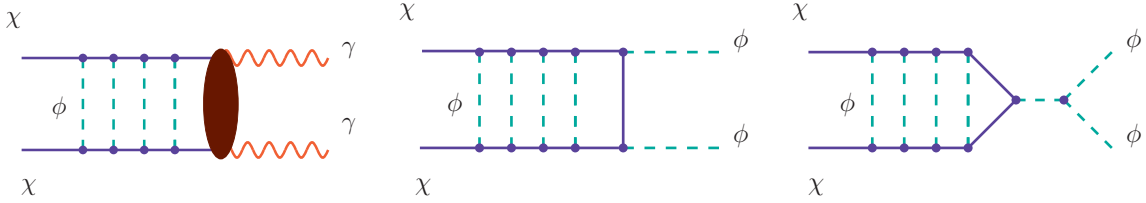


Figure 1: (Left) Feynman diagram of DM annihilation into  $2\gamma$  with multiple-exchange of force-carriers which leads to the Sommerfeld enhancement; (Middle) diagram of  $t$ -channel DM annihilation into force-carrier particles; (Right) diagram of  $s$ -channel DM particle annihilation into force-carrier particles through  $\phi^3$  type interactions.

## 2 Sommerfeld enhancements of $p$ -wave DM annihilation and thermal relic density

The Sommerfeld enhancement of annihilation cross-section occurs when the annihilating particles self-interact through a long-range attractive potential  $V(\mathbf{r})$  at low velocities [34]. In this scenario, the short-distance DM annihilation cross-section can be greatly enhanced due to the distortion of the wave functions of annihilating particles at origin [35–38]. The attractive potential may originate from multiple-exchange of light force carrier particles between the annihilating DM particles as shown in Fig. 1. The nature of Sommerfeld enhancement have been extensively studied (see, e.g., Refs. [39–48]) in light of the cosmic-ray positron/electron excesses observed by PAMELA [49], ATIC [50], and Fermi-LAT [51] etc..

In the previous studies, the force-carrier  $\phi$  is often assumed to be a vector boson, as it can be naturally light [39]. The maximally allowed enhancement factor turned out to be stringently constrained by the thermal relic density due to the additional  $s$ -wave annihilation  $\chi\chi \rightarrow \phi\phi$  in the presence of the light force-carrier  $\phi$ , which may challenge the Sommerfeld enhancement as an explanation for those excesses [47, 48, 52]. Note that the cosmic-ray lepton excesses may have astrophysical origins and may not be related to the halo DM annihilation. In this work, we shall consider the Sommerfeld enhancement as a mechanism to simultaneously account for both the possible gamma-ray line signals and the correct thermal relic density. For this purpose, we shall focus on the case of *scalar* force-carriers. Although in both the vector and scalar cases the induced long-range attractive potential is of the same Yukawa type. For a scalar force-carrier, the  $\chi\bar{\chi} \rightarrow \phi\phi$  is dominated by  $p$ -wave processes, which significantly modifies the relic density constraints due to the different velocity dependencies. The two-body wave function  $\Psi(\mathbf{r})$  of the

annihilating DM particles satisfies the non-relativistic Schrödinger equation

$$-\frac{1}{m_\chi}\nabla^2\Psi(\mathbf{r}) + V(\mathbf{r})\Psi(\mathbf{r}) = m_\chi v^2\Psi(\mathbf{r}), \quad (1)$$

where  $v = v_{\text{rel}}/2$  is the velocity of DM particle in the center-of-mass frame and  $v_{\text{rel}}$  is the relative velocity of the annihilating DM particles. After an expansion over angular momentum  $\ell$ , namely,  $\Psi(r, \theta) = \sum_\ell P_\ell(\cos \theta)\chi_\ell(r)/r$ , the Schrödinger equation for radial wave function  $\chi_\ell$  can be written as:

$$\frac{d^2\chi_\ell(t)}{dt^2} - \left[ \frac{\ell(\ell+1)}{t^2} + \frac{V(t)}{m_\chi v^2} \right] \chi_\ell(t) + \chi_\ell(t) = 0, \quad (2)$$

where  $t \equiv m_\chi v r$ . The above Schrödinger equation can be solved with the following boundary conditions [41, 42]

$$\lim_{t \rightarrow 0} \chi_\ell(t) = t^{\ell+1} \text{ and } \lim_{t \rightarrow \infty} \chi_\ell(t) \rightarrow C \sin\left(t - \frac{\ell\pi}{2} + \delta_\ell\right), \quad (3)$$

where  $\delta_\ell$  is the phase shift and  $C$  is a normalization constant. With the above boundary conditions, the Sommerfeld enhancement factor  $S_\ell$  of the annihilation cross-section is given by [39]

$$S_\ell \equiv \lim_{t \rightarrow 0} \left| \frac{\chi_\ell(t)}{\chi_\ell^{(0)}(t)} \right|^2 = \left[ \frac{(2\ell+1)!!}{C} \right]^2, \quad (4)$$

where  $\chi_\ell^{(0)}(t)$  is the wave function in the free-motion case without a potential. The exchange of massive vector or scalar particles  $\phi$  between the DM particles results in an attractive Yukawa potential

$$V(r) = -\frac{\alpha e^{-m_\phi r}}{r}, \quad (5)$$

where  $\alpha = g^2/(4\pi)$  is the coupling strength of  $\chi\bar{\chi}\phi$  or  $\bar{\chi}\gamma^\mu\chi\phi_\mu$  type of interactions. The nature of the Sommerfeld enhancement depends on the two variables

$$\epsilon_v \equiv \frac{v}{\alpha} \text{ and } \epsilon_\phi \equiv \frac{m_\phi}{\alpha m_\chi}. \quad (6)$$

In the limit of  $\epsilon_\phi \ll \epsilon_v^2$ , the Yukawa potential can be well approximated by a Coulomb-type potential. The corresponding Schrödinger equation can be solved analytically for arbitrary angular momentum and the enhancement factors are [42]

$$S_\ell^{\text{Col}} = \begin{cases} \left(\frac{\pi}{\epsilon_v}\right) \frac{1}{1 - \exp(-\pi/\epsilon_v)}, & (\text{for } \ell = 0), \\ S_0^{\text{Col}} \cdot \prod_{n=1}^{\ell} \left(1 + \frac{1}{4n^2\epsilon_v^2}\right), & (\text{for } \ell \neq 0). \end{cases} \quad (7)$$

For small  $\epsilon_v/\pi \ll 1$ , the enhancement factors can be approximated by  $S_\ell^{\text{Col}} \approx 2\pi/((2\epsilon_v)^{2\ell+1}(\ell!)^2)$ . Therefore, at low velocities the  $s$ - and  $p$ -wave Sommerfeld enhancement factor scales as  $1/v$  and  $(1/v^3)$  respectively.

In the case where  $\epsilon_\phi$  is non-negligible, the  $1/v$  behavior of  $s$ -wave cross-section breaks down. Through approximating the Yukawa potential by the Hulthén potential, the  $s$ -wave Sommerfeld enhancement factor can be estimated as [42, 43]

$$S_0 \approx \left(\frac{\pi}{\epsilon_v}\right) \frac{\sinh\left(\frac{2\pi\epsilon_v}{\pi^2\epsilon_\phi/6}\right)}{\cosh\left(\frac{2\pi\epsilon_v}{\pi^2\epsilon_\phi/6}\right) - \cos\left(2\pi\sqrt{\frac{1}{\pi^2\epsilon_\phi/6} - \frac{\epsilon_v^2}{(\pi^2\epsilon_\phi/6)^2}}\right)}. \quad (8)$$

For  $\epsilon_\phi \gg \epsilon_v$ , namely, the deBroglie wavelength of incoming particles is longer than the range of the interaction, the  $s$ -wave Sommerfeld enhancement saturate with  $S_0 \sim 12/\epsilon_\phi$ . But for some particular values of  $\epsilon_\phi \simeq 6/(\pi^2 n^2)$ , ( $n = 1, 2, 3, \dots$ ) for which the DM can form zero-energy bound states, there exists additional resonant enhancements which scale as  $1/v^2$ . The resonant enhancement is eventually cut off by the finite width of the resonance [39].

For  $p$ -wave Sommerfeld enhancement factor  $S_1$ , there is no analytic expression available. The  $p$ -wave case has been investigated in Refs. [40–42] without considering its effects on the freeze out and thermal relic density. In this work, we shall focus on these effects as they are important in determining the maximally allowed Sommerfeld enhancement. We first numerically solve the Eq. (2) with the boundary conditions in Eq. (3) and illustrate the dependence of  $S_1$  on the two variables  $\epsilon_v$  and  $\epsilon_\phi$  in Fig. 2. For small  $\epsilon_\phi \lesssim 10^{-3}$ , the value of  $S_1$  scales as  $1/v^3$  as expected from the Coulomb limit. For larger  $\epsilon_\phi$  in the range  $10^{-3} - 10^{-1}$ , it has resonant behavior which is similar to the  $s$ -wave case. For even larger  $\epsilon_\phi \gtrsim 10^{-1}$  the enhancement saturates. Note that the generic  $p$ -wave annihilation cross-section before including the Sommerfeld enhancement is proportional to  $v^2$ , thus the velocity dependence of the total Sommerfeld enhanced  $p$ -wave annihilation cross-section should be proportional to  $S_1\epsilon_v^2$ . In the right panel of Fig. 2, the contours of  $S_1\epsilon_v^2$  in the  $(\epsilon_v, \epsilon_\phi)$  plane are shown. In the region where  $\epsilon_\phi \lesssim 10^{-3}$ , it scales as  $1/v$  instead of  $1/v^3$ . In the resonance region  $10^{-3} \lesssim \epsilon_\phi \lesssim 10^{-1}$ , the velocity dependence of  $S_1\epsilon_v^2$  is not significant. In the saturation region  $\epsilon_\phi \gtrsim 10^{-1}$ ,  $S_1\epsilon_v^2$  scales as  $v^2$ , the total cross-section decreases rapidly towards low velocities. Thus the main difference from the  $s$ -wave case is that the total  $p$ -wave annihilation cross-section can be either velocity-suppressed or velocity-enhanced, depending on the size of  $\epsilon_\phi$ .

An important quantity directly related to the thermal relic density is thermally averaged annihilation cross-section. The generic DM annihilation cross-section times the relative velocity before including the Sommerfeld enhancement has the form  $(\sigma v_{\text{rel}})_0 =$

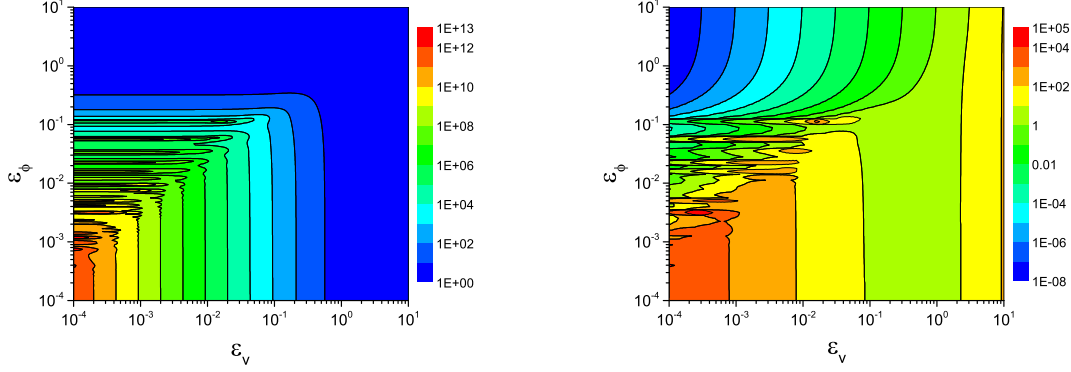


Figure 2: (Left) Contours of  $p$ -wave Sommerfeld enhancement  $S_1$  with Yukawa potential in  $(\epsilon_v, \epsilon_\phi)$  plane. (Right) the same but for  $S_1 \epsilon_v^2$  which is relevant to the total  $p$ -wave annihilation cross-section.

$a + bv_{\text{rel}}^2 + \mathcal{O}(v_{\text{rel}}^4)$ , where  $a$  and  $b$  are coefficients correspond to the  $s$ - and  $p$ -wave contributions which are velocity-independent. After including the Sommerfeld enhancement, the thermally averaged cross-section at a temperature  $T$  can be written as

$$\langle \sigma v_{\text{rel}} \rangle = a \langle S_0(v_{\text{rel}}) \rangle + b \langle v_{\text{rel}}^2 S_1(v_{\text{rel}}) \rangle, \quad (9)$$

where the thermal average of a quantity  $\mathcal{X}(v_{\text{rel}})$  in the non-relativistic limit is given by

$$\langle \mathcal{X} \rangle = \frac{x^{3/2}}{2\sqrt{\pi}} \int_0^\infty \mathcal{X}(v_{\text{rel}}) e^{-\frac{xv_{\text{rel}}^2}{4}} v_{\text{rel}}^2 dv_{\text{rel}}, \quad (10)$$

with  $x \equiv m_\chi/T$ . The thermally averaged annihilation cross-section is a function of  $x$  and depends on the parameters  $\alpha$  and  $m_\phi$ .

The time evolution of the DM number density  $n_\chi$  is governed by the Boltzmann equation

$$\frac{dn_\chi}{dt} + 3Hn_\chi = -\langle \sigma v_{\text{rel}} \rangle [n_\chi^2 - (n_\chi^{\text{eq}})^2], \quad (11)$$

where  $n_\chi^{\text{eq}}$  is the equilibrium DM number density and  $H$  is the Hubble constant. The equation is often rewritten as

$$\frac{dY}{dx} = -\sqrt{\frac{\pi}{45}} m_{\text{Pl}} m_\chi \frac{g_{*s} g_*^{-1/2}}{x^2} \langle \sigma v_{\text{rel}} \rangle [Y^2 - (Y^{\text{eq}})^2], \quad (12)$$

where  $Y^{(\text{eq})} \equiv n_\chi^{(\text{eq})}/s$  is the (equilibrium) number density rescaled by entropy density  $s$ ,  $m_{\text{Pl}} \simeq 1.22 \times 10^{19}$  GeV is the Planck mass scale.  $g_{*s}$  and  $g_*$  are the effective relativistic degrees of freedom for entropy and energy density respectively. The decoupling temperature  $x_f$  is defined as the temperature at which the dark matter particles start to depart

from the thermal equilibrium, and the density  $Y$  is related to the equilibrium density  $Y^{\text{eq}}$  by  $Y(x_f) \equiv (1+c)Y^{\text{eq}}(x_f)$ , where  $c$  is a constant of order unity. The value of  $x_f$  is approximately given by [53]

$$x_f \approx \ln[0.038c(c+2)m_{\text{Pl}}m_\chi(g_\chi g_*^{-1/2})\langle\sigma v_{\text{rel}}\rangle] - \frac{1}{2} \ln \ln[0.038c(c+2)m_{\text{Pl}}m_\chi(g_\chi g_*^{-1/2})\langle\sigma v_{\text{rel}}\rangle], \quad (13)$$

with  $g_\chi$  the degrees of freedom of dark matter particle. In the absence of Sommerfeld enhancement  $\langle\sigma v_{\text{rel}}\rangle = a + 6b/x_f$ , taking  $c \approx 1(2)$  for  $s(p)$ -wave annihilation leads to good fits to the numerical solutions of the Boltzmann equation. The DM number density in the present-day can be obtained by integrating Eq. (12) with respect to  $x$  in the region  $x_f \leq x \leq x_s$ , where  $x_s$  corresponds to the temperature at which the DM annihilation rate is insignificant compared with that of the expansion of the Universe and  $Y(x)$  becomes stable. The value of  $Y(x_s)$  can be written as

$$\frac{1}{Y(x_s)} = \frac{1}{Y(x_f)} + \sqrt{\frac{\pi}{45}} m_{\text{Pl}} m_\chi \int_{x_f}^{x_s} \frac{g_{*s} g_*^{-1/2}}{x^2} \langle\sigma v_{\text{rel}}\rangle dx. \quad (14)$$

In performing the integration over  $x$ , as  $\langle\sigma v_{\text{rel}}\rangle$  depends on temperature, one needs to take into account the effects of kinetic decoupling. When the DM particles are in both chemical and kinetic equilibrium with the radiation background, the temperature of the DM particles tracks that of the background, i.e.,  $T_\chi = T$  or  $x_\chi \equiv m_\chi/T_\chi = x$ . After dropping out of chemical equilibrium, the DM particles can still remain in kinetic equilibrium with the radiation background through scattering off SM relativistic particles which are in thermal equilibrium with the radiation background. At some temperature  $T_{\text{kd}}$ , when the rate of the scattering cannot compete with that of the expansion of the Universe, the DM particles start to decouple from kinetic equilibrium. After the kinetic decoupling,  $T_\chi$  drops quickly with the scale factor  $a$  as  $a^{-2}$  instead of  $a^{-1}$ , the temperatures of the DM particles and the radiation background are approximately related by  $T_\chi = T^2/T_{\text{kd}}$ , or  $x_\chi = x^2/x_{\text{kd}}$  [54]. Thus the integration from  $x_f$  to  $x_s$  needs to be separated into two parts, from  $x_f$  to  $x_{\text{kd}}$  and from  $x_{\text{kd}}$  to  $x_s$ . For the second part of the integration, one should use  $x_\chi$  instead of  $x$ . Previous analysis have shown that including the effect of kinetic decoupling leads to a significant reduction of relic density in the case of  $s$ -wave annihilation with Sommerfeld enhancement [45, 46, 48]. The value of  $T_{\text{kd}}$  is model-dependent, for instance, in supersymmetric models  $T_{\text{kd}} \approx 10^{-3} - 10^{-1} T_f$  [55]. In this work, we shall take the value of  $T_{\text{kd}}$  as a free parameter. Finally, after freeze out, the relic abundance of DM particles is given by

$$\Omega h^2 \approx 2.76 \times 10^8 Y(x_s) \left( \frac{m_\chi}{\text{GeV}} \right), \quad (15)$$



which is to be compared with the observed value  $\Omega h^2 = 0.113 \pm 0.004$  [56].

We solve the Boltzmann equation Eq.(12) numerically including the effects of Sommerfeld enhancement and kinetic decoupling for both  $s$ -wave and  $p$ -wave annihilation. In order to facilitate the comparison, we take  $a = 2.2 \times 10^{-26} \text{ cm}^3\text{s}^{-1}$  and  $b = 1.7 \times 10^{-25} \text{ cm}^3\text{s}^{-1}$  such that the final DM relic abundance  $\Omega h^2 \approx 0.112$  is the same for both  $s$ -wave and  $p$ -wave in the absence of Sommerfeld enhancement and kinetic decoupling. We fix  $m_\chi = 130 \text{ GeV}$  and  $m_\phi = 0.25 \text{ GeV}$  and consider two different values of  $\alpha = 0.1$  and  $0.01$ , and two kinetic decoupling temperatures  $T_f = 2T_{\text{kd}}$  and  $10T_{\text{kd}}$ . The evolutions of  $Y(x) - Y^{\text{eq}}(x)$  as a function of  $x$  are shown in Fig. 3. For both  $s$ - and  $p$ -wave annihilation, the inclusion of Sommerfeld enhancement results in reduction of final thermal relic density by a factor of  $\mathcal{O}(1)$ . For  $\alpha = 0.1$  the relic density is reduced by a factor of  $\sim 3$  for  $s$ -wave annihilation while  $\sim 2$  for  $p$ -wave case. At high temperatures  $x \sim 20$ , the  $p$ -wave annihilation cross-section still decreases with temperature in the presence of Sommerfeld enhancement, which leads to earlier decoupling from the thermal background and larger relic density. As it can be seen in Fig. 3, the effects of kinetic decoupling are significantly different between  $s$ - and  $p$ -wave case. For  $T_f = 2T_{\text{kd}}$  and  $10T_{\text{kd}}$ , the kinetic decoupling leads to further reduction of relic density by  $\sim 50\%$ ( $20\%$ ) in the  $s$ -wave case. However, for  $p$ -wave case, the reduction is almost invisible for  $\alpha = 0.1$  as shown in Fig. 3. For smaller  $\alpha = 0.01$ , it even leads to a slight enhancement of the relic density. This is because the kinetic decoupling makes the DM particle freeze out more quickly in the  $p$ -wave case as the annihilation cross-section decreases with temperature.

### 3 Sommerfeld enhancement of $\chi\bar{\chi} \rightarrow \gamma X$ cross-sections

As the force-carriers are much lighter than the DM particles, i.e.,  $m_\phi \ll m_\chi$ , the DM particles necessarily annihilate into the force carriers, which can be the dominant contribution to the thermal relic density. The process itself is also Sommerfeld-enhanced, which complicates the calculation of the relic density. Before including the Sommerfeld enhancement, the total DM annihilation cross-section  $(\sigma_{\text{tot}} v_{\text{rel}})_0$  can be written as

$$(\sigma_{\text{tot}} v_{\text{rel}})_0 = (\sigma_{\phi\phi} v_{\text{rel}})_0 + (\sigma_{\gamma X} v_{\text{rel}})_0. \quad (16)$$

The DM particles can always pair annihilate into  $\phi\phi$  through  $t$ -channel  $\chi$ -exchange. In addition, if there exists non-negligible cubic and quartic self-interactions between the force-carriers of the form  $-\mu\phi^3/3! - \lambda\phi^4/4!$ , there could be two-body or three-body  $s$ -channel annihilation. The three-body annihilation is suppressed by small phase-space and is neglected in the present work. For scalar force-carrier, both the  $t$ - and  $s$ -channel annihilation into  $\phi\phi$  are  $p$ -wave processes (see, Fig. 1). The total cross-section is given

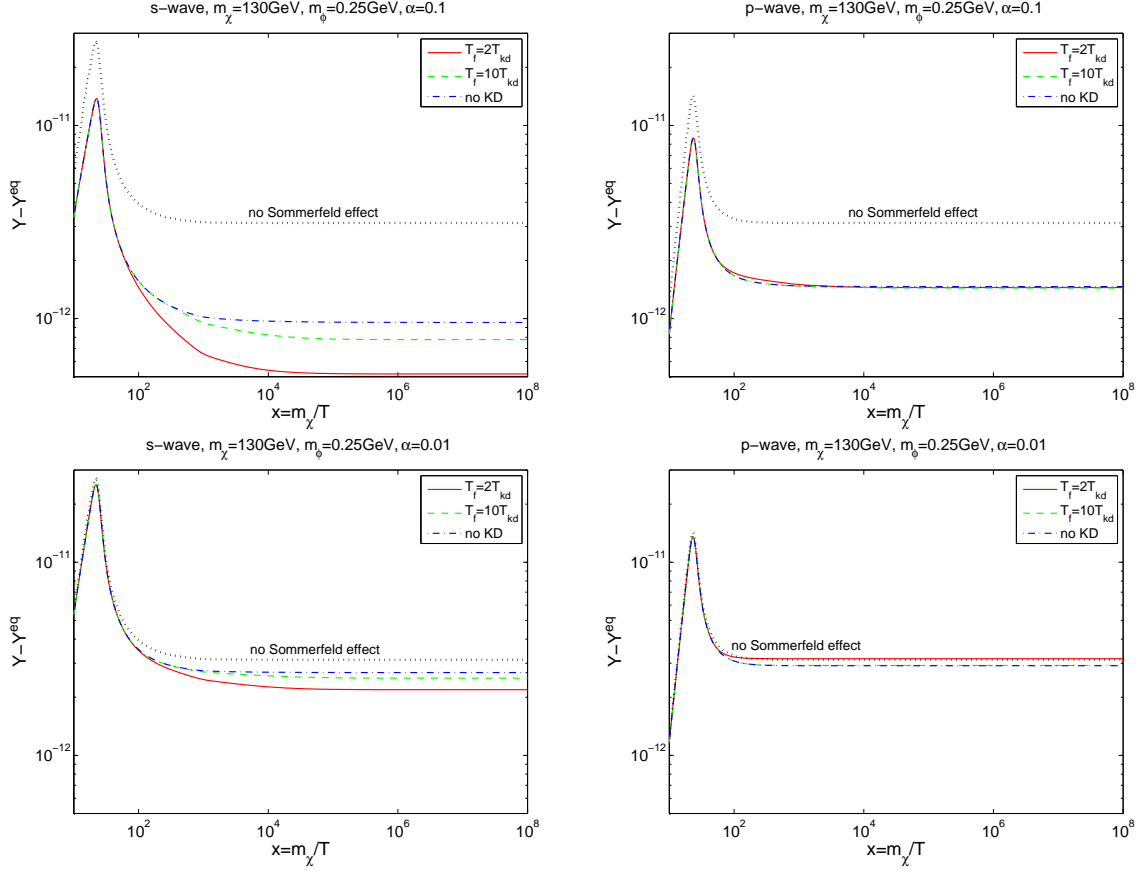


Figure 3: Effects of Sommerfeld enhancement and kinetic decoupling on the temperature evolution of the DM number density for the case of  $s$ -wave (left) and  $p$ -wave (right) with  $\alpha = 0.1$  and  $0.01$ , see text for explanations.

by

$$(\sigma_{\phi\phi}v_{\text{rel}})_0 = \frac{3\pi\alpha^2}{8m_\chi^2} \left( 1 - \frac{5}{18}\xi + \frac{1}{48}\xi^2 \right) v_{\text{rel}}^2, \quad (17)$$

with  $\xi = \mu/(2m_\chi\sqrt{\alpha\pi})$ . We assume that the annihilation of DM particles into  $\gamma X$  is an  $s$ -wave process such that there is no explicit velocity dependence in  $(\sigma_{\gamma X}v_{\text{rel}})_0$ . After including the Sommerfeld enhancement, the total thermally averaged annihilation cross-section is

$$\langle\sigma_{\text{tot}}v_{\text{rel}}\rangle = (\sigma_{\gamma X}v_{\text{rel}})_0\langle S_0\rangle + \langle(\sigma_{\phi\phi}v_{\text{rel}})_0 S_1\rangle. \quad (18)$$

The Sommerfeld enhancement factors  $S_{0,1}$  and the cross-section  $(\sigma_{\phi\phi}v_{\text{rel}})_0$  depend on  $\alpha$  and  $m_\phi$ . The requirement of reproducing the correct relic density constrains the size of  $\alpha$  for a given  $m_\phi$ , which in turn constrains the size of the Sommerfeld enhancement for  $\chi\bar{\chi} \rightarrow \gamma X$  today. In the left panel of Fig. 4, we show the allowed values of  $\alpha$  as a function of  $(\sigma_{\gamma\gamma}v_{\text{rel}})_0$  for various choices of  $\mu$  with fixed  $m_\phi = 0.25$  GeV. For very small

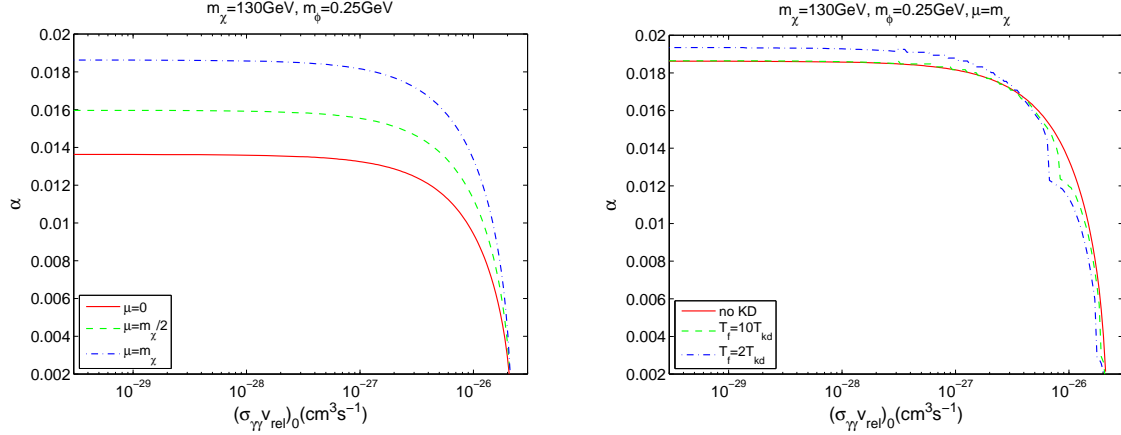


Figure 4: The value of  $\alpha$  allowed by the DM thermal relic density as a function of  $(\sigma_{\gamma\gamma}v_{\text{rel}})_0$ . (Left) the cases without kinetic decoupling. Three curves correspond to  $\mu = 0$  (solid),  $m_\chi/2$  (dashed), and  $m_\chi$  (dot-dashed), respectively. (Right) the case with kinetic decoupling. Three curves correspond to without kinetic decoupling (solid),  $T_{\text{kd}} = T_f/10$  (dashed) and  $T_f/2$  (dot-dashed), respectively with  $\mu$  fixed at  $m_\chi$ .

$(\sigma_{\gamma\gamma}v_{\text{rel}})_0 \ll 10^{-26} \text{ cm}^3\text{s}^{-1}$ , namely the total annihilation cross-section is dominated by  $(\sigma_{\phi\phi}v_{\text{rel}})_0$  at freeze out, the allowed value of  $\alpha$  is insensitive to  $(\sigma_{\gamma\gamma}v_{\text{rel}})_0$ . From the figure, one obtains  $\alpha \approx 0.0136, 0.0159$ , and  $0.0186$  for  $\mu = 0, m_\chi/2$ , and  $m_\chi$ , respectively. When  $(\sigma_{\gamma\gamma}v_{\text{rel}})_0$  increases and approaches  $\sim 10^{-26} \text{ cm}^3\text{s}^{-1}$ , the value of  $(\sigma_{\phi\phi}v_{\text{rel}})_0$  has to decrease rapidly in order to give the correct relic density, which leads to a significant reduction of  $\alpha$ . In the right panel of Fig. 4, the effects of kinetic decoupling are shown for  $T_f = 2T_{\text{kd}}$  and  $10T_{\text{kd}}$ . For small  $(\sigma_{\gamma\gamma}v_{\text{rel}})_0 \ll 10^{-26} \text{ cm}^3\text{s}^{-1}$ , the inclusion of kinetic decoupling leads to increment on the allowed value of  $\alpha$ , which is expected as in this region the  $p$ -wave annihilation dominates, making DM freeze out more quickly with kinetic decoupling as discussed in the previous section. For large  $(\sigma_{\gamma\gamma}v_{\text{rel}})_0 \sim 10^{-26} \text{ cm}^3\text{s}^{-1}$ , the effect of kinetic decoupling becomes significant, which leads to further decrease of  $\alpha$ . Some jumps in the curves are due to resonance of  $s$ -wave Sommerfeld effect.

After obtaining the allowed values of  $\alpha$ , the Sommerfeld enhancements at low velocities can be calculated straightforwardly. The Sommerfeld enhancement of the halo DM annihilation cross-section today is given by

$$\langle S_0 \rangle_{\text{now}} = \frac{1}{Nv_0^3} \sqrt{\frac{2}{\pi}} \int_0^{v_{\text{esc}}} S_0 e^{-\frac{v_{\text{rel}}^2}{2v_0^2}} v_{\text{rel}}^2 dv_{\text{rel}}, \quad (19)$$

where  $v_0$  is the DM velocity dispersion and  $v_{\text{esc}}$  is the DM escape velocity.  $N = \text{erf}(z/\sqrt{2}) - (2/\pi)^{1/2} ze^{-z^2/2}$  is a normalization constant with  $z = v_{\text{esc}}/v_0$ . Both  $v_{\text{esc}}$  and  $v_0$  depend on the distance  $r$  from the GC. In the vicinity of the Sun,  $r = r_\odot \approx 8.5$

kpc,  $v_{\text{esc}}(r_{\odot}) \approx 525 \text{ km s}^{-1}$  and  $v_0(r_{\odot}) \approx 210 \text{ km s}^{-1}$ . In the left panel of Fig. 5, we show dependence of  $\langle S_0 \rangle_{\text{now}}$  on the coupling  $\alpha$  and the velocity dispersion  $v_0$ .

For the allowed values  $\alpha = 0.0136, 0.0159$ , and  $0.0186$  corresponding to  $\mu = 0, m_{\chi}/2$ , and  $m_{\chi}$ , the enhancement factors are  $\langle S_0 \rangle_{\text{now}} \approx 170, 70$ , and  $50$ , respectively. Thus the enhancement factor can reach  $\mathcal{O}(100)$  with the constraints from DM thermal relic density, which is larger than that case where the force-carrier is a vector boson [47, 48]. In the right panel of Fig. 5, the relation between  $\langle \sigma_{\gamma\gamma} v_{\text{rel}} \rangle_{\text{now}}$  and  $(\sigma_{\gamma\gamma} v_{\text{rel}})_0$  is shown. In order to reproduce the observed signal corresponding to the cross-section around  $\langle \sigma_{\gamma\gamma} v_{\text{rel}} \rangle_{\text{now}} \approx 1.27 \times 10^{-27} \text{ cm}^3 \text{ s}^{-1}$  for the Einasto profile [2], the required cross-sections before the Sommerfeld enhancement are quite small  $(\sigma_{\gamma\gamma} v_{\text{rel}})_0 = 7.2 \times 10^{-30} \text{ cm}^3 \text{ s}^{-1}$ ,  $1.8 \times 10^{-29} \text{ cm}^3 \text{ s}^{-1}$ , and  $2.5 \times 10^{-29} \text{ cm}^3 \text{ s}^{-1}$ , respectively.

The cross-section of  $\chi\bar{\chi} \rightarrow \gamma X$  may be further enhanced due to the possible lower DM velocity dispersion near the GC. The dependence of Sommerfeld enhancement on  $v_0(r)$  or at GC has been discussed in Refs. [57, 58]. The N-body simulations suggest that  $v_0(r)$  is related to the DM density profile  $\rho(r)$  through a relation  $v_0(r)^3/\rho(r) \approx r^x$  [59]. From pure DM simulations the power index  $\chi \simeq 1.9 - 2.0$  [60]. For the NFW profile  $\rho(r) \propto (r/r_s)^{-\alpha} (1 + r/r_s)^{-3+\alpha}$  with  $\alpha = 1.0$  and  $r_s = 20 \text{ kpc}$ ,  $v_0(r)$  scales  $r^{x-\alpha}$ , thus it decreases with  $r$ . This is also true for the Einasto profile  $\rho(r) \propto \exp[-(2/\alpha)(r/r_s)^\alpha]$  if one takes the typical value  $\alpha = 0.17$ . Thus larger  $s$ -wave Sommerfeld enhancement at GC is expected. If the Sommerfeld enhancement saturates, it is insensitive to the choice of  $v_0(r)$ . The additional enhancement at GC can be estimated as  $S_0(v=0)/S_0(v_0(r_{\odot}))$  [61]. Note that the simulation results may be modified significantly after including baryons [62].

Although at freeze out  $\langle \sigma_{\phi\phi} v_{\text{rel}} \rangle$  can be a few order of magnitudes larger than  $\langle \sigma_{\gamma\gamma} v_{\text{rel}} \rangle$ , at low temperatures it is possible that  $\langle \sigma_{\gamma\gamma} v_{\text{rel}} \rangle$  is comparable with or even larger than  $\langle \sigma_{\phi\phi} v_{\text{rel}} \rangle$ , which is due to the dramatic difference in velocity dependencies between  $s$ - and  $p$ -wave processes. In Fig. 6, we show how  $\langle \sigma_{\phi\phi} v_{\text{rel}} \rangle$  and  $\langle \sigma_{\gamma\gamma} v_{\text{rel}} \rangle$  evolve with the variable  $x$ . At  $x = 25$ ,  $\langle \sigma_{\phi\phi} v_{\text{rel}} \rangle \approx 1 \times 10^{-25} \text{ cm}^3 \text{ s}^{-1}$  which is about four order of magnitudes larger than  $\langle \sigma_{\gamma\gamma} v_{\text{rel}} \rangle$ . When the temperature goes down, the value of  $\langle \sigma_{\phi\phi} v_{\text{rel}} \rangle$  decrease rapidly. The Sommerfeld enhancement of  $\langle \sigma_{\phi\phi} v_{\text{rel}} \rangle$  is significant in the range  $10^4 \leq x \leq 10^6$  as it is near a resonance region. For very large  $x \geq 10^8$ ,  $\langle \sigma_{\phi\phi} v_{\text{rel}} \rangle$  decrease monotonically. On the other hand, the value of  $\langle \sigma_{\gamma\gamma} v_{\text{rel}} \rangle$  increases towards large  $x$ . At  $x = 25$ ,  $\langle \sigma_{\gamma\gamma} v_{\text{rel}} \rangle \approx 10^{-29} \text{ cm}^3 \text{ s}^{-1}$ , at  $x \approx 4 \times 10^6$  which corresponds to  $v_0 = 210 \text{ km s}^{-1}$ , it reaches  $10^{-27} \text{ cm}^3 \text{ s}^{-1}$  and comes larger than  $\langle \sigma_{\phi\phi} v_{\text{rel}} \rangle$  for  $\mu = 0$  case. Thus, it is possible that  $\langle \sigma_{\gamma\gamma} v_{\text{rel}} \rangle$  can be the main DM annihilation channel, which is suggested by the current observations. Such a large enhancement is consistent with the limits derived from BBN and CMB data [63], as the total DM annihilation cross-section after the

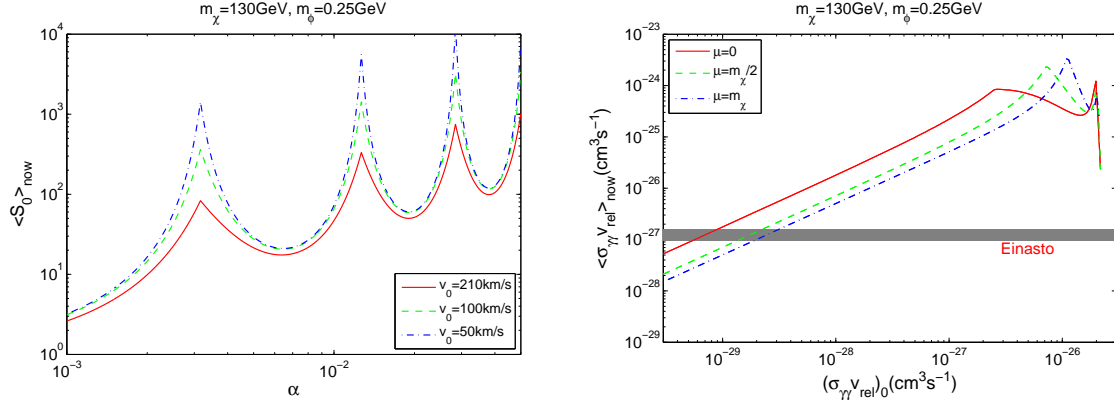


Figure 5: (Left)  $\langle S_0 \rangle_{\text{now}}$  as a function of coupling strength  $\alpha$  for the velocity dispersion  $v_0 = 210 \text{ km s}^{-1}$ ,  $100 \text{ km s}^{-1}$ , and  $50 \text{ km s}^{-1}$  respectively. (Right) the relation between  $\langle \sigma_{\gamma\gamma} v_{\text{rel}} \rangle_{\text{now}}$  and  $(\sigma_{\gamma\gamma} v_{\text{rel}})_0$  for three different values of  $\mu$ . The gray band denotes the fit cross-section  $\langle \sigma_{\gamma\gamma} v \rangle = (1.27 \pm 0.32) \times 10^{-27} \text{ cm}^3 \text{s}^{-1}$  in the case of Einasto profile [2]. Other parameters are fixed at  $m_\chi = 130 \text{ GeV}$  and  $m_\phi = 0.25 \text{ GeV}$ .

Sommerfeld enhancement is still an order of magnitude smaller than the typical WIMP annihilation cross-section.

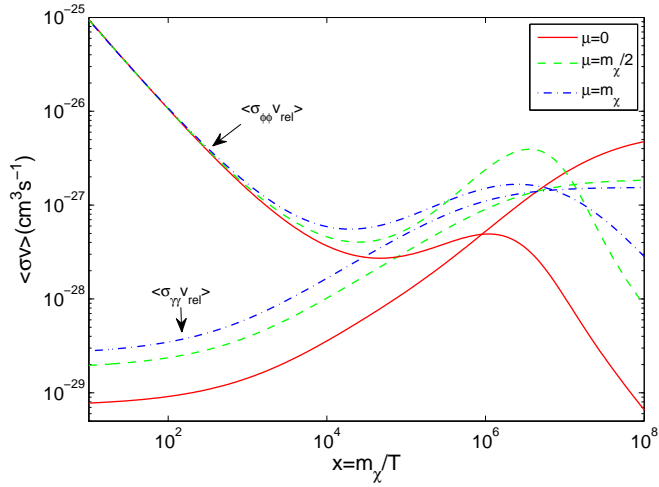


Figure 6: Temperature evolution of  $\langle \sigma_{\phi\phi} v_{\text{rel}} \rangle$  and  $\langle \sigma_{\gamma\gamma} v_{\text{rel}} \rangle$  for three different values of  $\mu = 0$ ,  $m_\chi/2$ , and  $m_\chi$ , respectively.

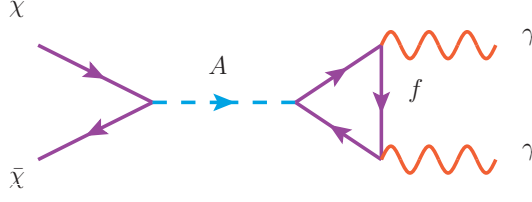


Figure 7: Feynman diagram for  $\chi\bar{\chi} \rightarrow \gamma\gamma$  through loop diagrams with an intermediate pseudoscalar  $A^0$  and a charged fermion  $f$  in the loop.

## 4 Sommerfeld enhancement in a simple model

In many DM models, the processes of DM annihilation into  $2\gamma$  proceed through loop diagrams which involve massive charged particles in the loop ( for exceptions, see, e.g. models in Ref. [64, 65] ). Due to the loop suppression, in general the DM effective couplings to the charged particles inside the loop have to be quite large in order to generate the observed cross-section around  $\mathcal{O}(10^{-27}\text{cm}^3\text{s}^{-1})$ , which may raise the problem of perturbativity. In the presence of Sommerfeld enhancements, the required coupling strength can be significantly reduced. In this section, we consider a realization of Sommerfeld enhancement in a simple reference model. In the model, the DM particle  $\chi$  is a Majorana fermion. Other particles in the models are: a light scalar force-carrier  $\phi$ , a heavy pseudoscalar mediator  $A^0$  and a heavy charged Dirac fermion  $f$  with electromagnetic charge number  $Q_f$  and color number  $C_f$ . The relevant interactions between the particles are given by the following Lagrangian

$$\mathcal{L}_{int} \subset -\frac{g}{2}\bar{\chi}\phi\chi - i\frac{g_\chi}{2}\bar{\chi}\gamma_5\chi A^0 - ig_f\bar{f}\gamma_5f A^0. \quad (20)$$

In order to avoid constraints from continuum photon spectrum, we consider the case where  $m_f, m_A \gg m_\chi$ , such that  $\chi\bar{\chi}$  can only annihilate into  $\gamma\gamma$  through one loop process as shown in Fig. 7.

The annihilation cross-section for this process is

$$(\sigma_{\gamma\gamma}v_{rel})_0 = \frac{1}{4\pi^3} \frac{\alpha_{em}^2 g_\chi^2 g_f^2 Q_f^4 C_f^2 m_f^2}{(s - m_A^2)^2 + m_A^2 \Gamma_A^2} \left[ \arctan \left( \frac{1}{\sqrt{m_f^2/m_\chi^2 - 1}} \right) \right]^4, \quad (21)$$

where  $s$  is the center-of-mass energy. The pseudoscalar  $A^0$  can decay into  $\chi\bar{\chi}$ ,  $f\bar{f}$  and  $\gamma\gamma$  with partial widths

$$\Gamma_{\chi\bar{\chi}} = \frac{g_\chi^2 m_A}{16\pi} \sqrt{1 - \frac{4m_\chi^2}{m_A^2}}, \quad \Gamma_{f\bar{f}} = \frac{g_f^2 m_A}{8\pi} \sqrt{1 - \frac{4m_f^2}{m_A^2}} \quad (22)$$

and

$$\Gamma_{\gamma\gamma} = \frac{m_A^3 \alpha_{em}^2 g_f^2 Q_f^4 C_f^2}{256 \pi^3 m_f^2} |A_{1/2}^A(m_A^2/4m_f^2)|^2, \quad (23)$$

where the function  $A_{1/2}^A$  is defined as  $A_{1/2}^A(\tau) = 2\tau^{-1}f(\tau)$  with

$$f(\tau) = \begin{cases} \arcsin^2 \sqrt{\tau} & (\text{for } \tau \leq 1) \\ -\frac{1}{4} \left( \ln \frac{1+\sqrt{1-1/\tau}}{1-\sqrt{1-1/\tau}} - i\pi \right)^2 & (\text{for } \tau > 1) \end{cases}.$$

We assume that in the dark sector the parity is conserved such that the decay  $A^0 \rightarrow \phi\phi$  is forbidden. As  $A^0$  is a pseudoscalar, the process  $\chi\bar{\chi} \rightarrow \gamma\gamma$  is an  $s$ -wave process. For heavy  $m_A, m_f \gg m_\chi$ , the size of the annihilation cross-section can be estimated as

$$(\sigma_{\gamma\gamma} v_{\text{rel}})_0 \approx 0.97 \times 10^{-27} \left( \frac{g_\chi g_f}{100} \right)^2 \left( \frac{m_\chi}{130 \text{ GeV}} \right)^4 \left( \frac{500 \text{ GeV}}{m_A} \right)^4 \left( \frac{500 \text{ GeV}}{m_f} \right)^2 \text{ cm}^3 \text{ s}^{-1}. \quad (24)$$

Thus typically a very large product of the couplings  $\sqrt{g_\chi g_f} \sim 10$  is required, which may invalidate the perturbative calculations.

One way to enhance the cross-section is to assume that the annihilation is near a resonance which occurs if  $m_A \approx 2m_\chi + \delta$  with  $\delta \ll m_A$ . In this case the cross-section can be enhanced by a factor of  $m_A^2/\Gamma_A^2$  with  $\Gamma_A$  the total width of  $A^0$ . If  $m_f$  is greater than  $2m_A$ , the total width can be estimated as  $\Gamma_A \approx \Gamma_{\chi\bar{\chi}}$  and the enhancement factor is  $\sim 32\pi^2 m_A/(g_A^2 \delta)$ . If small couplings  $g_A, g_f \approx 1$  is required, the relative mass difference should be around  $\delta/m_A \approx 3\%$ . Another modest enhancement may arise from the case where  $m_\chi \approx m_f$  such that the function  $\arctan[(m_f^2/m_\chi^2 - 1)^{-1/2}]$  reaches its maximal value  $\pi/2$ . Compared with the case where  $m_f \approx 5m_\chi$  the enhancement is  $\sim 8$ . In addition, in order to have the correct relic density, it is required that  $\delta > 0$  [18].

With the presence of Sommerfeld enhancements, the required couplings can be reduced significantly without introducing any mass degeneracies. In Fig. 8, we show the required couplings which can reproduce the observed  $\langle \sigma_{\gamma\gamma} v_{\text{rel}} \rangle = 1.27 \times 10^{-27} \text{ cm}^3 \text{ s}^{-1}$ . Compared with the case without Sommerfeld enhancements, the required products  $g_\chi g_f$  can be reduced by an order of magnitude. For a wide range of the pseudoscalar mass  $100 < m_{A^0} < 450 \text{ GeV}$ , the required couplings are smaller than unity. If the Sommerfeld enhancements are absent, only a narrow region close to  $2m_\chi$  can be consistent with a small  $g_\chi g_f$ .

## 5 Conclusions

In summary, the recently reported possible indications of line spectral features in the Fermi-LAT photon spectrum in regions close to the galactic center can be related to the

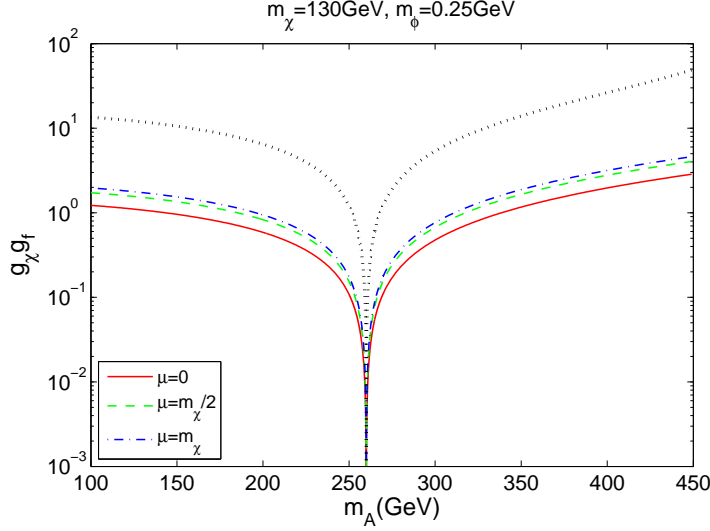


Figure 8: The required value of  $g_\chi g_f$  to account for the gamma-ray line signals with cross-section  $\langle \sigma_{\gamma\gamma} v \rangle = 1.27 \times 10^{-27} \text{cm}^3 \text{s}^{-1}$  [2]. Three cases with Sommerfeld enhancement correspond to  $\mu = 0$  (solid),  $m_\chi/2$  (dashed), and  $m_\chi$  (dot-dashed), respectively. The dotted line denotes the case without Sommerfeld enhancement. Other parameters are fixed at  $Q_f = C_f = 1$ ,  $g_\chi = g_f$ , and  $m_f = 300 \text{ GeV}$ .

signals of halo DM annihilation. However, the corresponding annihilation cross-section of  $\langle \sigma_{\gamma\gamma} v_{\text{rel}} \rangle \approx \mathcal{O}(10^{-27}) \text{cm}^3 \text{s}^{-1}$  is too large for typical loop-induced radiative processes, while on the other hand too small to be responsible for the observed DM relic density which is typically  $3 \times 10^{-26} \text{cm}^3 \text{s}^{-1}$ . We have pointed out that the Sommerfeld enhancement with scalar force-carrier can simultaneously explain those features. In this mechanism, the cross-section for DM annihilation into  $\gamma X$  in the galactic center today can be greatly enhanced due to the attractive forces between the DM particles, which is induced by the multiple-exchange of the force-carriers. The additional  $p$ -wave annihilation into the force-carriers can dominate the total DM annihilation cross-section at freeze out and set the correct thermal relic density, but can have subdominant contributions to the DM annihilation today due to the velocity suppression. We have performed an detailed analysis on the allowed Sommerfeld enhancement under the constraints from the thermal relic density determined by  $p$ -wave annihilation processes. The results show that the Sommerfeld enhancement factor can reach  $\mathcal{O}(100)$ . In a simple model with  $\chi\bar{\chi} \rightarrow 2\gamma$  occurring at one loop level, we have shown that the required DM effective couplings to the intermediate particles in the loop can be reduced by an order of magnitude and close to unity, which keeps the perturbativity. Compared with some other mechanisms for increasing the DM annihilation cross-section at loop level, the Sommerfeld enhancement



does not require any degeneracies in the masses of DM particles and the intermediate particles in the loop diagrams.

## Acknowledgments

This work is supported in part by the National Basic Research Program of China (973 Program) under Grants No. 2010CB833000; the National Nature Science Foundation of China (NSFC) under Grants No. 10975170, No. 10821504 and No. 10905084; and the Project of Knowledge Innovation Program (PKIP) of the Chinese Academy of Science.

## References

- [1] T. Bringmann, X. Huang, A. Ibarra, S. Vogl, and C. Weniger, *Fermi LAT Search for Internal Bremsstrahlung Signatures from Dark Matter Annihilation*, *JCAP* **1207** (2012) 054, [[arXiv:1203.1312](#)].
- [2] C. Weniger, *A Tentative Gamma-Ray Line from Dark Matter Annihilation at the Fermi Large Area Telescope*, *JCAP* **1208** (2012) 007, [[arXiv:1204.2797](#)].
- [3] E. Tempel, A. Hektor, and M. Raidal, *Fermi 130 GeV gamma-ray excess and dark matter annihilation in sub-haloes and in the Galactic centre*, *JCAP* **1209** (2012) 032, [[arXiv:1205.1045](#)].
- [4] A. Rajaraman, T. M. Tait, and D. Whiteson, *Two Lines or Not Two Lines? That is the Question of Gamma Ray Spectra*, *JCAP* **1209** (2012) 003, [[arXiv:1205.4723](#)].
- [5] M. Su and D. P. Finkbeiner, *Strong Evidence for Gamma-ray Line Emission from the Inner Galaxy*, [arXiv:1206.1616](#).
- [6] A. Hektor, M. Raidal, and E. Tempel, *An evidence for indirect detection of dark matter from galaxy clusters in Fermi-LAT data*, [arXiv:1207.4466](#).
- [7] M. Su and D. P. Finkbeiner, *Double Gamma-ray Lines from Unassociated Fermi-LAT Sources*, [arXiv:1207.7060](#).
- [8] D. Hooper and T. Linden, *Are Lines From Unassociated Gamma-Ray Sources Evidence For Dark Matter Annihilation?*, [arXiv:1208.0828](#).
- [9] A. Hektor, M. Raidal, and E. Tempel, *Double gamma-ray lines from unassociated Fermi-LAT sources revisited*, [arXiv:1208.1996](#).

- [10] N. Mirabal, *The Dark Knight Falters*, [arXiv:1208.1693](#).
- [11] Fermi-LAT Collaboration, <http://fermi.gsfc.nasa.gov/science/mtgs/symposia/2012/program/fri/AAlbert.pdf>, The Fermi Symposium, October 2012.
- [12] A. Boyarsky, D. Malyshev, and O. Ruchayskiy, *Spectral and spatial variations of the diffuse gamma-ray background in the vicinity of the Galactic plane and possible nature of the feature at 130 GeV*, [arXiv:1205.4700](#).
- [13] F. Aharonian, D. Khangulyan, and D. Malyshev, *Cold ultrarelativistic pulsar winds as potential sources of galactic gamma-ray lines above 100 GeV*, [arXiv:1207.0458](#).
- [14] A. Hektor, M. Raidal, and E. Tempel, *Fermi-LAT gamma-ray signal from Earth Limb, systematic detector effects and their implications for the 130 GeV gamma-ray excess*, [arXiv:1209.4548](#).
- [15] D. P. Finkbeiner, M. Su, and C. Weniger, *Is the 130 GeV Line Real? A Search for Systematics in the Fermi-LAT Data*, [arXiv:1209.4562](#).
- [16] M. R. Buckley and D. Hooper, *Implications of a 130 GeV Gamma-Ray Line for Dark Matter*, *Phys.Rev.* **D86** (2012) 043524, [[arXiv:1205.6811](#)].
- [17] S. Tulin, H.-B. Yu, and K. M. Zurek, *Three Exceptions for Thermal Dark Matter with Enhanced Annihilation to  $\gamma\gamma$* , [arXiv:1208.0009](#).
- [18] Y. Bai and J. Shelton, *Gamma Lines without a Continuum: Thermal Models for the Fermi-LAT 130 GeV Gamma Line*, *JHEP* **1212** (2012) 056, [[arXiv:1208.4100](#)].
- [19] W. Buchmuller and M. Garny, *Decaying vs Annihilating Dark Matter in Light of a Tentative Gamma-Ray Line*, *JCAP* **1208** (2012) 035, [[arXiv:1206.7056](#)].
- [20] T. Cohen, M. Lisanti, T. R. Slatyer, and J. G. Wacker, *Illuminating the 130 GeV Gamma Line with Continuum Photons*, *JHEP* **1210** (2012) 134, [[arXiv:1207.0800](#)].
- [21] I. Cholis, M. Tavakoli, and P. Ullio, *Searching for the continuum spectrum photons correlated to the 130 GeV gamma-ray line*, *Phys.Rev.* **D86** (2012) 083525, [[arXiv:1207.1468](#)].

- [22] X.-Y. Huang, Q. Yuan, P.-F. Yin, X.-J. Bi, and X.-L. Chen, *Constraints on the dark matter annihilation scenario of Fermi 130 GeV  $\gamma$ -ray line emission by continuous gamma-rays, Milky Way halo, galaxy clusters and dwarf galaxies observations*, *JCAP* **1211** (2012) 048, [[arXiv:1208.0267](#)].
- [23] M. Asano, T. Bringmann, G. Sigl, and M. Vollmann, *The 130 GeV gamma-ray line and generic dark matter model building constraints from continuum gamma rays, radio and antiproton data*, [arXiv:1211.6739](#).
- [24] E. Dudas, Y. Mambrini, S. Pokorski, and A. Romagnoni, *Extra  $U(1)$  as natural source of a monochromatic gamma ray line*, *JHEP* **1210** (2012) 123, [[arXiv:1205.1520](#)].
- [25] J. M. Cline, *130 GeV dark matter and the Fermi gamma-ray line*, *Phys.Rev.* **D86** (2012) 015016, [[arXiv:1205.2688](#)].
- [26] H. M. Lee, M. Park, and W.-I. Park, *Fermi Gamma Ray Line at 130 GeV from Axion-Mediated Dark Matter*, *Phys.Rev.* **D86** (2012) 103502, [[arXiv:1205.4675](#)].
- [27] B. Kyae and J.-C. Park, *130 GeV Gamma-Ray Line from Dark Matter Decay*, *Phys.Lett.* **B718** (2013) 1425–1429, [[arXiv:1205.4151](#)].
- [28] X. Chu, T. Hambye, T. Scarna, and M. H. Tytgat, *What if Dark Matter Gamma-Ray Lines come with Gluon Lines?*, *Phys.Rev.* **D86** (2012) 083521, [[arXiv:1206.2279](#)].
- [29] Z. Kang, T. Li, J. Li, and Y. Liu, *Brightening the (130 GeV) Gamma-Ray Line*, [arXiv:1206.2863](#).
- [30] J. H. Heo and C. Kim, *Cosmic ray signatures of Dipole-Interacting Fermionic Dark Matter*, [arXiv:1207.1341](#).
- [31] J.-C. Park and S. C. Park, *Radiatively decaying scalar dark matter through  $U(1)$  mixings and the Fermi 130 GeV gamma-ray line*, *Phys.Lett.* **B718** (2013) 1401–1406, [[arXiv:1207.4981](#)].
- [32] N. Weiner and I. Yavin, *UV Completions of Magnetic Inelastic Dark Matter and RayDM for the Fermi Line(s)*, [arXiv:1209.1093](#).
- [33] K. Schmidt-Hoberg, F. Staub, and M. W. Winkler, *Enhanced diphoton rates at Fermi and the LHC*, *JHEP* **1301** (2013) 124, [[arXiv:1211.2835](#)].
- [34] A. Sommerfeld, *Annalen der Physik*, 403, 257 (1931).

- [35] J. Hisano, S. Matsumoto, and M. M. Nojiri, *Unitarity and higher-order corrections in neutralino dark matter annihilation into two photons*, *Phys. Rev.* **D67** (2003) 075014, [[hep-ph/0212022](#)].
- [36] J. Hisano, S. Matsumoto, and M. M. Nojiri, *Explosive dark matter annihilation*, *Phys. Rev. Lett.* **92** (2004) 031303, [[hep-ph/0307216](#)].
- [37] J. Hisano, S. Matsumoto, M. M. Nojiri, and O. Saito, *Non-perturbative effect on dark matter annihilation and gamma ray signature from galactic center*, *Phys. Rev.* **D71** (2005) 063528, [[hep-ph/0412403](#)].
- [38] M. Cirelli, A. Strumia, and M. Tamburini, *Cosmology and Astrophysics of Minimal Dark Matter*, *Nucl. Phys.* **B787** (2007) 152–175, [[arXiv:0706.4071](#)].
- [39] N. Arkani-Hamed, D. P. Finkbeiner, T. R. Slatyer, and N. Weiner, *A Theory of Dark Matter*, *Phys.Rev.* **D79** (2009) 015014, [[arXiv:0810.0713](#)].
- [40] R. Iengo, *Sommerfeld enhancement for a Yukawa potential*, [arXiv:0903.0317](#).
- [41] R. Iengo, *Sommerfeld enhancement: general results from field theory diagrams*, *JHEP* **05** (2009) 024, [[arXiv:0902.0688](#)].
- [42] S. Cassel, *Sommerfeld factor for arbitrary partial wave processes*, *J. Phys.* **G37** (2010) 105009, [[arXiv:0903.5307](#)].
- [43] T. R. Slatyer, *The Sommerfeld enhancement for dark matter with an excited state*, *JCAP* **1002** (2010) 028, [[arXiv:0910.5713](#)].
- [44] A. Hryczuk, R. Iengo, and P. Ullio, *Relic densities including Sommerfeld enhancements in the MSSM*, *JHEP* **1103** (2011) 069, [[arXiv:1010.2172](#)].
- [45] J. B. Dent, S. Dutta, and R. J. Scherrer, *Thermal Relic Abundances of Particles with Velocity-Dependent Interactions*, *Phys.Lett.* **B687** (2010) 275–279, [[arXiv:0909.4128](#)].
- [46] J. Zavala, M. Vogelsberger, and S. D. White, *Relic density and CMB constraints on dark matter annihilation with Sommerfeld enhancement*, *Phys.Rev.* **D81** (2010) 083502, [[arXiv:0910.5221](#)].
- [47] J. L. Feng, M. Kaplinghat, and H.-B. Yu, *Halo Shape and Relic Density Exclusions of Sommerfeld-Enhanced Dark Matter Explanations of Cosmic Ray Excesses*, *Phys.Rev.Lett.* **104** (2010) 151301, [[arXiv:0911.0422](#)].

- [48] J. L. Feng, M. Kaplinghat, and H.-B. Yu, *Sommerfeld Enhancements for Thermal Relic Dark Matter*, *Phys.Rev.* **D82** (2010) 083525, [[arXiv:1005.4678](#)].
- [49] **PAMELA Collaboration** Collaboration, O. Adriani *et. al.*, *An anomalous positron abundance in cosmic rays with energies 1.5-100 GeV*, *Nature* **458** (2009) 607–609, [[arXiv:0810.4995](#)].
- [50] J. Chang *et. al.*, *An excess of cosmic ray electrons at energies of 300-800 GeV*, *Nature* **456** (2008) 362–365.
- [51] **Fermi LAT Collaboration** Collaboration, A. A. Abdo *et. al.*, *Measurement of the Cosmic Ray  $e^+$  plus  $e^-$  spectrum from 20 GeV to 1 TeV with the Fermi Large Area Telescope*, *Phys.Rev.Lett.* **102** (2009) 181101, [[arXiv:0905.0025](#)].
- [52] D. P. Finkbeiner, L. Goodenough, T. R. Slatyer, M. Vogelsberger, and N. Weiner, *Consistent Scenarios for Cosmic-Ray Excesses from Sommerfeld-Enhanced Dark Matter Annihilation*, *JCAP* **1105** (2011) 002, [[arXiv:1011.3082](#)].
- [53] R. J. Scherrer and M. S. Turner, *On the Relic, Cosmic Abundance of Stable Weakly Interacting Massive Particles*, *Phys.Rev.* **D33** (1986) 1585.
- [54] T. Bringmann and S. Hofmann, *Thermal decoupling of WIMPs from first principles*, *JCAP* **0407** (2007) 016, [[hep-ph/0612238](#)].
- [55] T. Bringmann, *Particle Models and the Small-Scale Structure of Dark Matter*, *New J.Phys.* **11** (2009) 105027, [[arXiv:0903.0189](#)].
- [56] **WMAP Collaboration** Collaboration, E. Komatsu *et. al.*, *Seven-Year Wilkinson Microwave Anisotropy Probe (WMAP) Observations: Cosmological Interpretation*, *Astrophys.J.Suppl.* **192** (2011) 18, [[arXiv:1001.4538](#)].
- [57] M. Cirelli and J. M. Cline, *Can multistate dark matter annihilation explain the high-energy cosmic ray lepton anomalies?*, *Phys.Rev.* **D82** (2010) 023503, [[arXiv:1005.1779](#)].
- [58] K. N. Abazajian and J. P. Harding, *Constraints on WIMP and Sommerfeld-Enhanced Dark Matter Annihilation from HESS Observations of the Galactic Center*, *JCAP* **1201** (2012) 041, [[arXiv:1110.6151](#)].
- [59] E. Bertschinger, *Astrophys.J. Suppl.* **58**, 39 (1985).
- [60] J. F. Navarro, A. Ludlow, V. Springel, J. Wang, M. Vogelsberger, *et. al.*, *The Diversity and Similarity of Cold Dark Matter Halos*, [arXiv:0810.1522](#).

- [61] T. R. Slatyer, N. Toro, and N. Weiner, *Sommerfeld-enhanced annihilation in dark matter substructure: Consequences for constraints on cosmic-ray excesses*, *Phys.Rev.* **D86** (2012) 083534, [[arXiv:1107.3546](#)].
- [62] P. B. Tissera, S. D. White, S. Pedrosa, and C. Scannapieco, *Dark matter response to galaxy formation*, [arXiv:0911.2316](#).
- [63] J. Hisano, M. Kawasaki, K. Kohri, T. Moroi, K. Nakayama, *et. al.*, *Cosmological constraints on dark matter models with velocity-dependent annihilation cross section*, *Phys.Rev.* **D83** (2011) 123511, [[arXiv:1102.4658](#)].
- [64] E. Dudas, Y. Mambrini, S. Pokorski, and A. Romagnoni, *Extra  $U(1)$  as natural source of a monochromatic gamma ray line*, *JHEP* **1210** (2012) 123, [[arXiv:1205.1520](#)].
- [65] N. Weiner and I. Yavin, *UV Completions of Magnetic Inelastic Dark Matter and RayDM for the Fermi Line(s)*, [arXiv:1209.1093](#).